Journal of Cell Science 108, 2781-2790 (1995)
Printed in Great Britain © The Company of Biologists Limited 1995

Protein translation components are colocalized in granules in oligodendrocytes

Elisa Barbarese[1], Dennis E. Koppel[2], Murray P. Deutscher[2], Candra L. Smith[3], Kevin Ainger[2], Frank Morgan[2] and John H. Carson[2,*]

[1]Department of Neurology, [2]Department of Biochemistry, [3]MD/PhD Program, University of Connecticut Health Center, Farmington, CT 06030, USA

*Author for correspondence

SUMMARY

The intracellular distribution of various components of the protein translational machinery was visualized in mouse oligodendrocytes in culture using high resolution fluorescence in situ hybridization and immunofluorescence in conjunction with dual channel confocal laser scanning microscopy. Arginyl-tRNA synthetase, elongation factor 1a, ribosomal RNA, and myelin basic protein mRNA were all co-localized in granules in the processes, veins and membrane sheets of the cell. Colocalization was evaluated by dual channel cross correlation analysis to determine the correlation index (% colocalization) and correlation distance (granule radius), and by single granule ratiometric analysis to determine the distribution of the different components in individual granules. Most granules contained synthetase, elongation factor, ribosomal RNA and myelin basic protein mRNA. These results indicate that several different components of the protein synthetic machinery, including aminoacyl-tRNA synthetases, elongation factors, ribosomes and mRNAs, are colocalized in granules in oligodendrocytes. We propose that these granules are supramolecular complexes containing all of the necessary macromolecular components for protein translation and that they represent a heretofore undescribed subcellular organization of the protein synthetic machinery. This spatial organization may increase the efficiency of protein synthesis and may also provide a vehicle for transport and localization of specific mRNAs within the cell.

Key words: confocal, correlation analysis, in situ hybridization, aminoacyl-tRNA synthetase, elongation factor, ribosome, mRNA

INTRODUCTION

Protein synthesis involves sequential molecular interactions among a variety of different macromolecular components including: mRNA, ribosomes, tRNAs, aminoacyl-tRNA synthetases and a variety of initiation, elongation and release factors. Several lines of evidence indicate that in eucaryotic cells many of these components are structurally and spatially organized (Ryazonov et al., 1987; Negrutskii et al., 1994). Biochemical studies indicate that mRNA (Biegel and Pachter, 1991; Cervera et al., 1981; Pachter, 1992; Singer, 1992; Taneja et al., 1992), polyribosomes (Lenk et al., 1977; Howe and Hershey, 1984), aminoacyl-tRNA synthetases (Dang et al., 1983; Mirande et al., 1985), initiation factors (Howe and Hershey, 1984) and elongation factors (Mirande et al., 1985) are associated with the cytoskeletal matrix. Complexes between aminoacyl-tRNA synthetases (Deutscher, 1984; Mirande et al., 1985), mRNA (Miseta et al., 1991), ribosomes (Graf, 1976; Irvin and Hardesty, 1972) and elongation factors (Bec et al., 1989) have also been isolated biochemically. Functional studies provide evidence for 'channeling' of aminoacyl-tRNA during protein synthesis in vivo (Negrutskii and Deutscher, 1991), and for sequestering of aminoacyl-tRNA (Negrutskii and Deutscher, 1992), implying structural organization of these components within the cell. Morphological studies indicate spatial localization of certain mRNAs to specific subcellular regions in a variety of different systems (Singer, 1992). This is generally assumed to reflect a mechanism to achieve spatially restricted translation of the localized mRNA within the cell, implying that components of the protein synthetic machinery are co-localized with the mRNAs. Thus, there is extensive biochemical, metabolic and morphological evidence for structural and spatial organization of the protein synthetic machinery in a variety of systems. However, the structural and spatial relationships of the various components of the protein synthetic machinery have not been visualized directly in intact cells.

In the work described here we have visualized the subcellular spatial distribution of several components of the protein synthetic machinery, including: arginyl-tRNA synthetase (ATS), elongation factor 1a (EF1a), ribosomal RNA (rRNA) and myelin basic protein (MBP) mRNA, in oligodendrocytes in primary culture. The unique morphology of these cells facilitates visualization of cytoplasmic components. The cell body

is quite small with several processes radiating out and expanding into an extensive array of membranous sheets, spanning several thousand μm^2. The sheets contain a continuous thin layer of cytoplasm with a network of branching veins. The entire cell, except for the nucleus and its immediate perikaryon, is flattened, with very little dimension in the *z*-axis. Thus, oligodendrocytes in culture display a broad expanse of cytoplasm and membrane in a very thin layer. This geometry tends to disperse intracellular components in the plane of the cell resulting in optical properties which are ideal for high resolution microscopy.

In addition to the excellent optical properties of the system, several myelin-specific mRNAs are expressed at high levels and are induced at defined stages of differentiation. Most of the mRNAs that have been analyzed in oligodendrocytes are confined to the perikaryon. However, MBP mRNA is localized to the peripheral processes and membranes elaborated by these cells. This has been demonstrated by subcellular fractionation (Colman et al., 1982), and in situ hybridization in brain (Trapp et al., 1987) and in culture (Holmes et al., 1988). Recently, we reported that both endogenous and exogenous MBP mRNA appear in granules that are associated with the cytoskeletal matrix in the processes and membranes of oligodendrocytes (Ainger et al., 1993). The work described here extends these observations by providing new information concerning the biochemical composition of the MBP mRNA-containing granules. The subcellular distribution of ATS, EF1a, rRNA and MBP mRNA was analyzed in detergent-extracted oligodendrocytes in order to facilitate visualization of granules. The distribution of ATS and EF1a was visualized by immunofluorescence (IF). The distribution of rRNA and MBP mRNA was visualized by fluorescent in situ hybridization (FISH). Colocalization of different components was measured in dual channel images using cross correlation analysis. The distribution of different components in individual granules was determined by ratiometric analysis.

MATERIALS AND METHODS

Cells

Brains from newborn (P0-P2) B6C3F2 mice (originally obtained from The Jackson Laboratories, Bar Harbor, ME) were used to generate primary glial cell cultures. The protocol was approved by the Animal Care Committee of UCHC in accordance with federally approved guidelines for the use of animals in research. Oligodendrocytes were isolated after 12-14 days of growth in culture as described previously (Barbarese, 1991; Ainger et al., 1993). Cells were extracted with detergent (Triton X-100) as described by Biegel and Pachter (1991) and fixed with paraformaldehyde or methanol for fluorescence in situ hybridization (FISH) and immunofluorescence (IF).

Chemicals

Tissue culture reagents were from Gibco (Gaithersburg, MD). Unless stated otherwise all other chemicals were from Sigma Chemical Co. (St. Louis, MO).

Fluorescence in situ hybridization

Digoxigenin-labeled and biotin-labeled probes for FISH were prepared by random oligonucleotide priming (Feinberg and Vogelstein, 1983) according to the manufacturer's instructions (Boehringer Mannheim, Indianapolis, IN, and Enzo Diagnostics, Farmingdale, NY, respectively). The MBP mRNA probe was prepared from a 1.5 kb *Eco*RI fragment of the rat 14 kDa MBP cDNA (Roach et al., 1983) cloned into a Bluescript II vector (Stratagene, La Jolla, CA). The rRNA probe was prepared from a 1.5 kb *Eco*RI fragment of clone HHCSA65 containing human 18 S ribosomal RNA, obtained from the ATCC (Rockville, MD). FISH was performed according to the protocol of Singer et al. (1986) as described previously (Ainger et al., 1993). The following negative controls were performed for each probe: sample digested with RNase, no probe, DNase-digested probe, non-homologous DNA (vector sequence) probe, no first antibody, no second antibody. In the case of MBP mRNA, additional negative controls were: oligodendrocytes from homozygous shiverer mice, which do not express MBP mRNA because of a deletion in the MBP gene, and astrocytes and fibroblasts, which occasionally contaminate the oligodendrocyte cultures and do not express MBP mRNA.

Immunofluorescence

Labeling for EF1a and ATS was performed on fixed cells after treatment with methanol (Dang et al., 1983). Goat anti-EF1a, obtained from Dr William Merrick (Case Western Reserve), was raised against purified EF1a, and recognized a single component by Ouchterlony and western blotting analysis. The serum was not fractionated. Rabbit anti-ATS, prepared as described previously (Vellkamp and Deutscher, 1987), was raised against purified ATS and recognized a single component by western blotting analysis. The serum was not fractionated. Rabbit anti-MBP, prepared as described previously (Barbarese et al., 1977), was raised against purified mouse 14 kDa MBP and recognized the four major MBP isoforms by western blotting. The antibody was affinity purified. Mouse monoclonal antibody to 2′3′-cyclic nucleotide phosphohydrolase (CNPase), obtained from Sigma (St. Louis, MO), was raised against purified CNPase and characterized by ELISA, western blotting and immunohistochemistry. It recognizes both isoforms of CNPase. Rabbit anti-tubulin, obtained from Accurate (Westbury, NY), was characterized by western blotting and immunohistochemistry. Texas Red- and fluorescein-conjugated goat anti-rabbit, goat anti-mouse, and mouse anti-goat antibodies were obtained from Organon-Teknica (Durham, NC), and used at 1:100 final dilution. Negative IF controls included: antiserum preadsorbed with purified antigen, no first antibody and no secondary antibody. RNA was visualized in live cells using SYTO 12 (5 nM in phosphate-free medium) obtained from Molecular Probes (Eugene, OR).

Confocal microscopy

Samples processed by FISH and/or IF were visualized by confocal microscopy using an Axiophot microscope (Zeiss, Oberkochen, Germany) with an MRC 600 confocal laser scanning system (BioRad, Hercules, CA). Images were collected using either a Nikon 60×, 1.4 N.A. objective or a Zeiss 40×, 0.75 N.A. objective. Texas Red and fluorescein images were collected simultaneously using excitation at 514 nm with appropriate discriminatory emission filters. Bleed-through of fluorescein signal into the red channel was corrected. There was no significant bleed-through of Texas Red signal into the green channel. For visualization, dual channel images were merged, maintaining full 8 bit dynamic range in each image, and displayed with red/green pseudocolor, using an SGI IRIS 340 VGX graphics workstation (Silicon Graphics, Inc., Mountain View, CA).

Dual channel cross correlation analysis

Colocalization of components in dual channel images was analyzed by dual channel cross correlation analysis to determine the correlation index and correlation distance. The regions of the image selected for analysis contained areas of the cell where granules were well resolved. Regions of the image outside the boundaries of the cell which were devoid of granules and regions over the cell body and nucleus, where the high density of granules and signal intensity degraded resolution, were masked out. Cross correlation analysis was performed as follows. Given two confocal images of the same cell (A(*m*,*n*) and B(*m*,*n*), where *m* and *n* correspond to the rows and

columns, respectively, in the two images), a cell mask $\sigma(m,n)$ is defined, which is 0 for all points outside the cell or in the cell body where granules overlap, and 1 for all points inside the cell where individual granules are well resolved. A cross correlation function $g(m',n')$ is then defined as follows:

$$g(m',n') = \frac{G_{AB}(m',n')}{[G_{AA}(0,0)G_{BB}(0,0)]^{1/2}} \quad (1)$$

where

$$G_{AB}(m',n') = \frac{\sum_{m''}\sum_{n''} \sigma(m'',n'')A(m'',n'')\sigma(m''+m',n''+n')B(m''+m',n''+n')}{\sum_{m''}\sum_{n''} \sigma(m'',n'')\sigma(m''+m',n''+n')} - \langle\sigma A\rangle\langle\sigma B\rangle \quad (2)$$

Using C to stand for A or B in equation (1) it follows that:

$$G_{CC}(0,0) = \langle(\sigma C)^2\rangle - \langle\sigma C\rangle^2 \quad (3)$$

where

$$\langle(\sigma C)^a\rangle = \frac{\sum_m\sum_n [\sigma(m,n)C(m,n)]^a}{\sum_m\sum_n [\sigma(m,n)]^a} \quad (4)$$

where a equals 1 for the second term on the right side in equation (3), and 2 for the first term. Correlation functions, defined as in equation (1), were displayed as surface plots.

The method was validated using two sets of control images. First, two different theoretical randomized images were cross-correlated with each other. The cross correlation values were close to 0 at every position including position 0,0 (data not shown). This indicates that the two images were completely random with respect to each other. Second, a single channel image of an oligodendrocyte containing granules was correlated with itself. The cross correlation values were dispersed in a Gaussian distribution with a maximum value of 1 at position 0,0 and decreasing values at positions displaced from 0,0, indicating a finite correlation distance (data not shown).

The correlation index is defined as the square root of the amplitude of the Gaussian distribution at position (0,0). This corresponds to the percentage colocalization (100% in the case of an image correlated with itself). The correlation distance is defined as the radius of the Gaussian distribution. This corresponds to the radius of the correlated objects (in this case granules) in the original image.

In order to determine the amplitude and radius of the cross correlation functions, granules were assumed to represent Gaussian shaped objects. Examination of the insets in Fig. 1 indicates that this is a reasonable assumption for most granules although some individual granules display non-Gaussian profiles. The images within the cell mask were then modeled as a distribution of Gaussian shaped objects of varying intensities giving the following relationship:

$$g(n\Delta x, m\Delta y) = \gamma^2 \exp\{-[(n\Delta x/R)^2+(m\Delta y/R)^2]\}+\beta \quad (5)$$

where γ is the correlation index (% colocalization), β is a small correction factor to the model, and R is the correlation distance of the Gaussian function (the average size of individual granules when measured to the $1/e^2$ point). The values from the cross correlation functions were fitted to theoretical Gaussian curves using the MLAB programming system (Civilized Software Inc., Bethesda MD). The amplitudes and radii were determined from the fitted curves.

To calculate the error of the cross correlation analysis, the following approach was used. For each image pair (proportional to a_i, b_i) in a dual channel data set, the N pixels in the analyzed area of the image were subsampled into M subgroups. This was done by placing sequential pixels into different subgroups such that group 1 contained pixels (i+1, i+M+1, i+2M+1...), group 2 contained pixels (i+2, i+M+2, i+2M+2...) and group M contained pixels (i+M, i+2M, i+3M...). The number of pixels, j, in each subgroup is equal to N/M. To control for possible artifacts related to the number of subgroups, subsampling was performed for values of M from 5 to 20.

For each subgroup (from 1 to M) the product of the deviations from the mean for the two images was calculated as shown:

$$f^{(1)} = \frac{1}{N/M}\sum_{j=1}^{N/M}\left[a_j^{(1)} - \frac{1}{N/M}\sum_{j=1}^{N/M} a_j^{(1)}\right]\left[b_j^{(1)} - \frac{1}{N/M}\sum_{j=1}^{N/M} b_j^{(1)}\right]$$
$$\vdots$$
$$f^{(M)} = \frac{1}{N/M}\sum_{j=1}^{N/M}\left[a_j^{(M)} - \frac{1}{N/M}\sum_{j=1}^{N/M} a_j^{(M)}\right]\left[b_j^{(M)} - \frac{1}{N/M}\sum_{j=1}^{N/M} b_j^{(M)}\right] \quad (6)$$

For each value of M, the arithmetic average ($\bar{f}$) over all the subgroups was calculated as shown in equation (7):

$$\bar{f} = \frac{1}{M}\sum_{k=1}^{M} f^{(k)} \quad (7)$$

The standard deviation (S) for each value of M was calculated as shown in equation (8):

$$S^{(M)} = \left[\frac{\sum_{k=1}^{M}[f^{(k)}]^2 - M\bar{f}^2}{M-1}\right]^{1/2} \quad (8)$$

The standard deviation divided by the arithmetic average for all values of M (from 5 to 20) was calculated as shown in equation (9):

$$\frac{S}{\bar{f}} = \frac{1}{\bar{f}}\sum_{M=5}^{20} S^{(M)} \quad (9)$$

Thus the correlation index is defined as:

$$\left[\gamma^2\left(\frac{S}{1\pm\bar{f}}\right)\right]^{1/2} \simeq \gamma\left(1 \pm \frac{S}{2\bar{f}}\right). \quad (10)$$

Single granule ratiometric analysis

In order to analyze the distributions of various components in individual granules, single granule ratiometric analysis was performed as follows. The coordinates of each well-resolved granule were determined by selecting the center or brightest pixel associated with the granule in one channel and selecting the corresponding coordinates in the second channel. Both channels were examined to ensure that granules that appeared in only one channel as well as granules that appeared in both channels were selected. The total intensity in each channel for each granule was determined from the sum of the pixel values for the central pixel and the 24 neighboring pixels (this being the approximate area occupied by most granules). The ratio value for each granule was calculated by dividing the total intensity in the green channel by the sum of the total intensities in the green and red channels. Thus, granules which are primarily labeled in the red channel with little label in the green channel appear red in the merged image and have low ratio values (<30%). Granules which are

primarily labeled in the green channel with little label in the red channel appear green and have high ratio values (>70%). Granules which are labeled in both channels appear yellow and have intermediate ratio values (30-70%). The intensity ratios were calculated for several hundred granules from at least five different cells and displayed as frequency distributions.

RESULTS

Fig. 1 illustrates some morphological features of oligodendrocytes in primary culture. Cells were stained with antibodies to a variety of different subcellular components including: a plasma membrane protein (MBP), a cytoplasmic protein (CNPase) and a cytoskeletal protein (tubulin). In addition, live cells were incubated with the vital nucleic acid stain, SYTO 12, which preferentially labels RNA. Each of these different subcellular components displays a characteristic pattern of distribution when visualized by immunofluorescence in fixed cells or by fluorescence in live cells. In the MBP-stained cell (panel A) the plasma membrane, including the membrane sheets, is clearly delineated. In the CNPase-stained cell (panel B) the cytoplasm in the perikaryon and processes is labeled. In the tubulin-stained cell (panel B) microtubule bundles in the processes and veins are labeled. In the SYTO 12-labeled cell

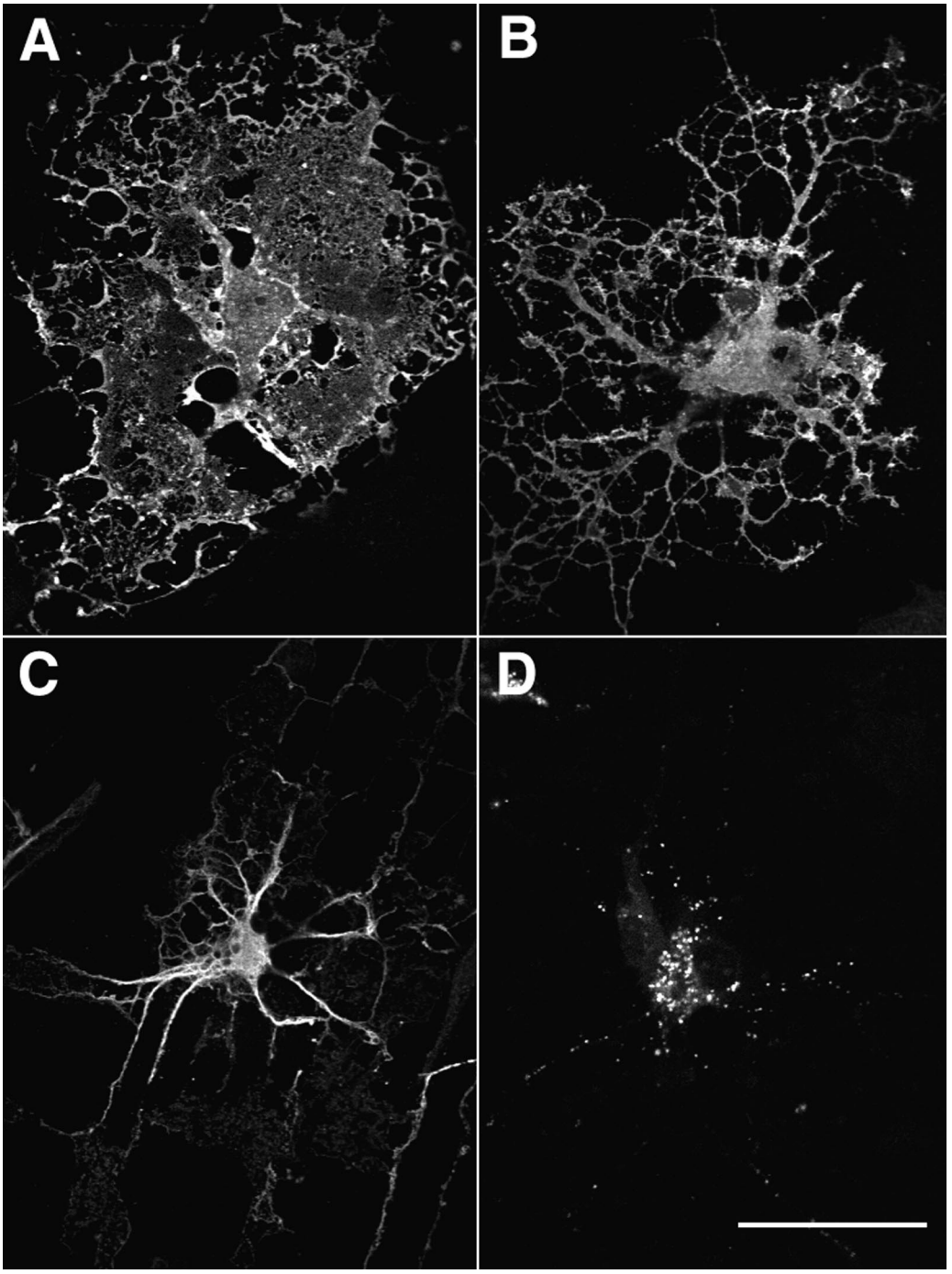

Fig. 1. Immunofluorescent labeling for MBP, CNPase and tubulin in fixed oligodendrocytes and RNA labeling in live cells. Oligodendrocytes were grown in culture and either fixed for IF or transferred to phosphate-free medium for RNA labeling. IF for MBP (A), CNPase (B) and tubulin (C) and SYTO 12 labeling for RNA (D) were performed as described in Materials and Methods. Fluorescence was imaged by confocal microscopy. Bar in D, 50 μm.

(panel D) discrete granules are detected in the perikaryon and processes indicating that RNA-containing granules exist in live cells.

ATS, EF1a, rRNA and MBP mRNA are localized in granules

Fig. 2 shows the intracellular distribution of various components of the protein synthetic machinery in oligodendrocytes. The images in Fig. 2 were collected at higher magnification than the images in Fig. 1 in order to resolve intracellular details. Cells were double-labeled for various pairwise combinations of protein synthetic components and the dual channel confocal data was displayed as red/green merged images. Fig. 2A shows a merged image of an oligodendrocyte double-labeled for ATS (green channel) and EF1a (red channel). Numerous granules are visible in the peripheral processes and membrane sheets of the cell. Clusters of granules appear to accumulate at branch points (inset). The majority of the granules appear yellow, indicating that they contain both ATS and EF1a. Very few of the granules appear green (ATS with little EF1a) or red (EF1a with little ATS). In the perikaryon, the labeling appears granular, but the density of labeling makes it difficult to resolve individual granules. In the nucleus, which appears as an acentrically positioned ovoid, the labeling is diffuse and the color is orange, indicating the presence of both EF1a and ATS, with EF1a present in higher amounts relative to ATS compared to the granules. These results indicate that EF1a and ATS are localized in granules in the oligodendrocyte cytoplasm and dispersed in the nucleus. Most of the well-resolved granules in the periphery of the cell appear to contain both EF1a and ATS.

Fig. 2B shows a merged image of an oligodendrocyte double labeled for ATS (green channel) and rRNA (red channel). Numerous granules are visible in the peripheral processes and membrane sheets of the cell. Most of the granules appear yellow, indicating the presence of both ATS and rRNA. However, a small population of granules appears green (ATS with little rRNA). Very few granules appear red (rRNA with little ATS). The perikaryon appears granular, but individual granules are not resolved. The nucleus appears green with large orange areas, indicating diffuse nuclear localization of ATS with concentrations of rRNA in specific areas (presumably nucleoli). The rRNA labeling intensity was greatly reduced when cells were pretreated with ribonuclease, and was absent when probe was omitted or when non-homologous probe was used (data not shown). Taken together, A and B indicate that there is a large population of granules in the periphery of the oligodendrocyte that contains ATS, EF1a and rRNA. A small population of granules contains ATS (and presumably EF1a, since most ATS-containing granules also contain EF1a) without rRNA.

Fig. 2C shows a merged image of an oligodendrocyte double labeled for ATS (green) and MBP mRNA (red). As in A and B there is a large number of ATS-containing granules in the periphery of the cell. Most of the ATS-containing granules appear yellow, indicating the presence of MBP mRNA, but some appear green (ATS with little MBP mRNA). Very few granules appear red (MBP mRNA with little ATS). The nucleus of the cell appears diffusely green (ATS without MBP mRNA). These results indicate that most of the MBP mRNA-containing granules in the oligodendrocyte also contain ATS (and presumably EF1a, see above).

In order to determine the proportion of MBP mRNA that associated with granules, the amount of MBP mRNA in extracted and unextracted cells was measured by northern blotting (data not shown). The results indicate that greater than 90% of the MBP mRNA in the oligodendrocyte remains associated with the cytoskeletal matrix after detergent extraction. Since the FISH signal in the extracted cells is localized almost exclusively to granules this means that most of the MBP mRNA in the cell is localized in granules. MBP mRNA labeling was not detected in oligodendrocytes from homozygous shiverer mice, which have a deletion in the MBP gene; nor in astrocytes and fibroblasts, which do not express MBP; nor in RNase-treated cells or cells incubated with non-homologous probe (data not shown).

Fig. 2D shows a merged image of an oligodendrocyte double labeled for rRNA (green) and MBP mRNA (red). There is a large number of rRNA-containing granules in the periphery of the cell. Some contain MBP mRNA and appear yellow while some do not contain MBP mRNA and appear green. In addition, there is a population of MBP mRNA-containing granules that do not contain rRNA and they appear red. The nucleus of the cell appears diffusely green (rRNA with little MBP mRNA) with areas of higher intensity corresponding to nucleoli. These results indicate that most MBP mRNA-containing granules also contain rRNA.

Dual channel cross correlation analysis of colocalization

The data in Fig. 2A-D indicate that ATS, EF1a, rRNA and MBP mRNA are all localized in granules in the periphery of the oligodendrocyte and suggest that in many cases the various components are colocalized. However, it is important to determine if the apparent colocalization is significant or due to random overlap of separate granules because of the density of granules in the peripheral cytoplasm. In order to distinguish between these two possibilities, dual channel cross correlation analysis of the red and green channel data from Fig. 1 was performed. Fig. 3A-D shows cross correlation functions calculated from the dual channel data from Fig. 2A-D. In each case the values show a Gaussian distribution with a maximum at position 0,0 in the center of the plot.

Two summary statistics, the correlation index and the correlation distance, were determined for each image pair by fitting theoretical Gaussian curves to the cross correlation data. The correlation index, defined as the square root of the amplitude of the cross correlation function, provides a measure of the percentage colocalization in the two images. The correlation distance, defined as the radius of the Gaussian distribution in the cross correlation function, provides a measure of the size of colocalized structures (in this case granules) in the original image. The values for the correlation index and correlation distance calculated from the correlation functions in Fig. 3 are given in Table 1. In the case of ATS and EF1a, the correlation index is (85±3)% and the correlation distance is 0.8 μm. In the case of ATS and rRNA, the correlation index is (75±2)% and the correlation distance is 0.6 μm. In the case of ATS and MBP mRNA the correlation index is (67 ±2)% and the correlation distance is 0.7 μm. In the case of rRNA and MBP mRNA the correlation index is (66±3)% and the correlation distance is 0.7 μm. These results demonstrate that the colocalization of ATS, EF1a, rRNA and MBP mRNA in

granules in oligodendrocytes is significant and that the mean granule radius is between 0.6 and 0.8 μm.

Size measurements based on fluorescence microscopy images are subject to inherent uncertainty due to the point spread function of the optical system. A sub-resolution fluor-escent bead (which can be considered a point source) produces an image profile of measurable size depending on its brightness. This can lead to overestimation of the actual size of the bead. Similar effects cause uncertainty in delineating the edges of larger fluorescent objects. Confocal microscopy minimizes this problem but does not eliminate it entirely. Therefore, there is some uncertainty in the estimated size of the granules. However, since the image profile of a single granule is considerably larger than the image profile of a sub-resolution bead, the uncertainty in size measurement due to the point spread function is relatively small compared to the overall size of the granule.

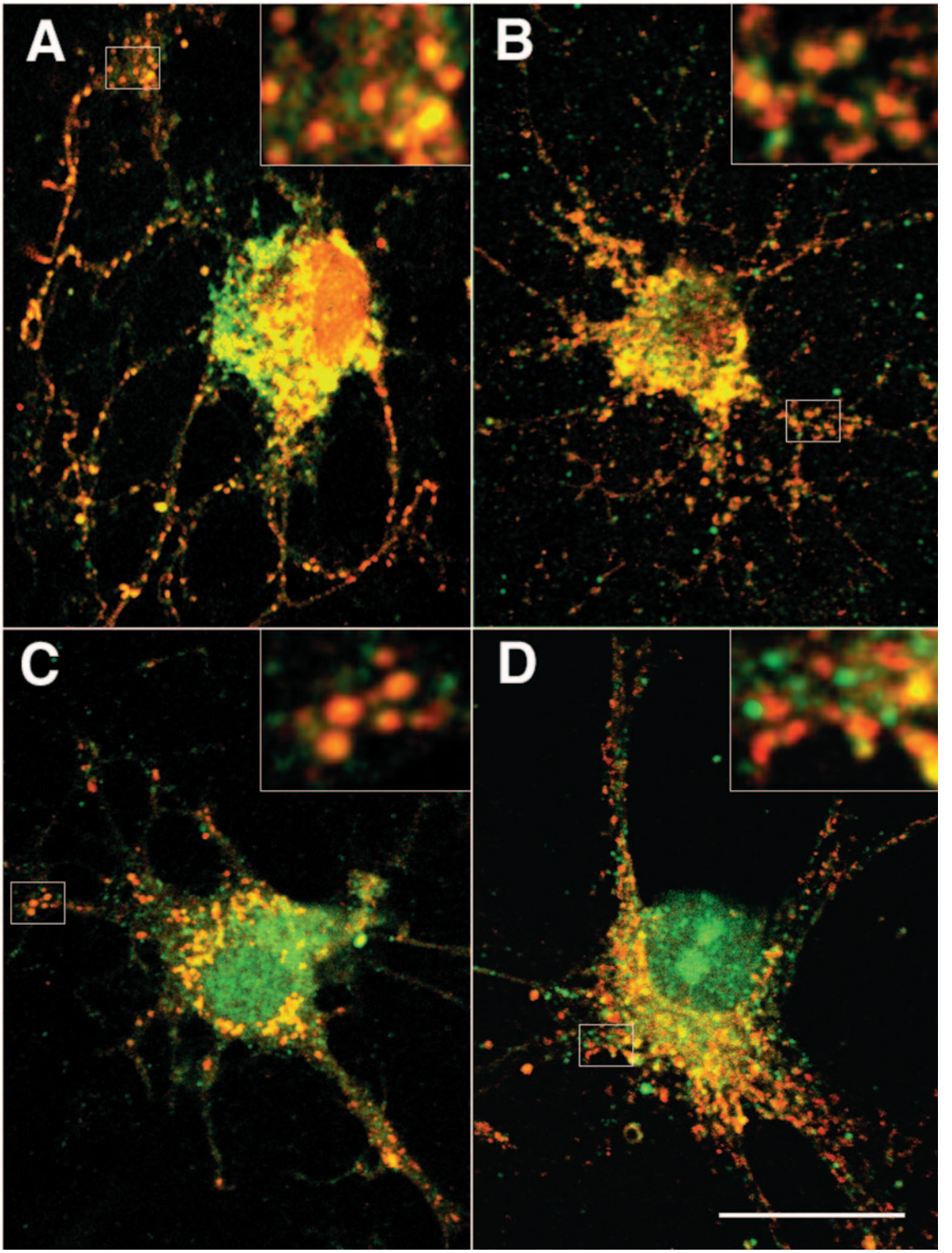

Fig. 2. Localization of ATS, EF1a, rRNA and MBP mRNA in granules in detergent-extracted oligodendrocytes. Oligodendrocytes were grown in culture, detergent extracted, fixed and prepared for double label IF or FISH. The two fluorophores (fluorescein and Texas Red) were visualized by dual channel confocal microscopy and merged images were rendered as described in Materials and Methods. Bar in D, 25 μm. The insets in the upper right of each panel show a cluster of granules (indicated by the small box) magnified 4× over the original image. (A) ATS (green channel)/EF1a (red channel). (B) ATS (green channel)/rRNA (red channel). (C) ATS (green channel)/MBP mRNA (red channel). (D) rRNA (green channel)/MBP mRNA (red channel).

Single granule ratiometric analysis of colocalization

The dual channel cross correlation analysis described above demonstrates that oligodendrocytes contain a population of granules in which ATS, EF1a, rRNA and MBP mRNA are colocalized. However, examination of the color of individual granules in the images in Fig. 2 reveals that some granules appear to be deficient in specific components. In order to analyze the distribution of the various components in individual granules, single granule ratiometric analysis was performed. The frequency distributions of ratiometric values for individual granules are shown in Fig. 4. This analysis is limited to well-resolved granules in the periphery of the cell. Granules in the perikaryon are not sufficiently well resolved to measure the intensities in individual granules and thus they are not included in the analysis. In EF1a/ATS-labeled cells (Fig. 4A) virtually all of the labeled granules appear yellow, with ratios between 45 and 65%, indicating that they contain both components. This means that the ratio of EF1a to ATS is relatively uniform among different granules. In rRNA/ATS-labeled cells (Fig. 4B) there appear to be two populations of granules: a major group that appears yellow, with ratios between 30 and 65%, containing both components; and a minor group that appears green, with ratios >65%, containing ATS (and presumably EF1a, since these components are highly colocalized) but deficient in rRNA. In MBP mRNA/ATS-labeled cells (Fig. 4C) there also appear to be two populations of granules: a major group that appears yellow, with ratios between 30 and 65%, containing both components; and a minor group that appears geen with ratios between >65%, which contains ATS (and presumably EF1a) but is deficient in MBP mRNA. In MBP mRNA/rRNA-labeled cells (Fig. 4D) there appear to be three populations of granules: one major group that appears yellow, with ratios between 30 and 70%, containing both components; and two minor groups, one that appears red, with ratios <30%, containing MBP mRNA, but lacking rRNA, and a second that appears green, with ratios >70%, containing rRNA, but lacking MBP mRNA.

DISCUSSION

The results reported here indicate that in oligodendrocytes at least four components of the protein synthetic machinery: ATS, EF1a, rRNA and MBP mRNA are colocalized in structures which appear as granules in detergent-extracted cells. Since there is extensive biochemical, metabolic and morphological evidence that various components of the protein synthetic machinery associate with each other and with the cytoskeletal matrix, we propose that all of the essential components of the translational apparatus are present in these granules, including: mRNA, ribosomes, multiple tRNAs and aminoacyl-tRNA synthetases, and various initiation, elongation and release factors necessary for protein synthesis. Thus, the protein synthetic machinery of the cell appears to be organized into supramolecular complexes (granules).

If the granules contain all of the components necessary for protein synthesis they must be relatively large. In fact, cross correlation analysis indicates a correlation distance (or granule radius) of approximately 0.7 μm. The size of a single ribosome (the single most massive granule component identified in this study) is approximately 30 nm. Thus, a single granule is large enough to accommodate several hundred ribosomes. The fact that the size of the ribosome-deficient granules appears the same as the ribosome-containing granules suggests that the

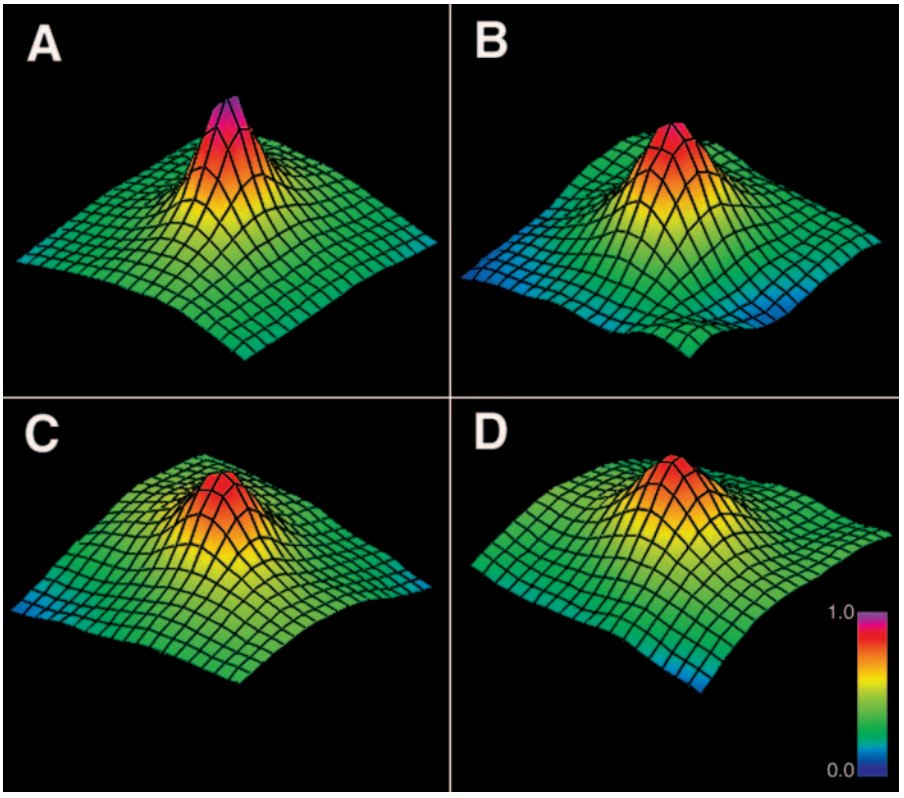

Fig. 3. Dual channel cross correlation analysis of colocalization. Cross correlation functions were calculated for the separate red and green channel images from Fig. 1. (A-D) correspond to Fig. 1A-D, respectively. The functions are displayed as surface plots with the individual points shown as vertices on an overlaid grid. Each square on the grid represents a displacement of one pixel in the original image. The central point corresponds to the 0,0 position in each plot. The value of the function at each point is plotted from 0.0 to 1.0 on the *z*-axis and mapped to the color lookup table shown in the lower right-hand corner of D.

Table 1. Correlation index and distance for different correlation functions

Correlation function	Correlation index (%)	Correlation distance (μm)
EF1a/ATS	85±3	0.8
rRNA/ATS	75±2	0.6
MBP mRNA/ATS	67±2	0.7
MBP mRNA/rRNA	66±3	0.7

The values from the cross correlation functions in Fig. 3 (A-D, for EF1a/ATS, rRNA/ATS, MBP mRNA/ATS and MBP mRNA/rRNA, respectively) were fitted to theoretical Gaussian curves as described in Materials and Methods. The amplitudes and radii were determined from the fitted curves. The correlation index is defined as the square root of the amplitude of the Gaussian distribution at position (0,0). This corresponds to the percentage colocalization of the two labeled components. The correlation distance is defined as the radius of the Gaussian distribution. This corresponds to the radius of the correlated objects in the original image.

structural organization of the granule is determined by components other than ribosomes.

The apparent size of the granules raises the question of why such large subcellular structures have not been reported previously. There are several possible explanations. Conventional light and electron microscopic techniques are optimized for visualizing membranous intracellular organelles. The granules are apparently not enclosed in membrane vesicles because their components are retained after extraction with non-ionic detergent. Therefore, they may be difficult to visualize by conventional microscopic techniques. Electron microscopy of longitudinal sections of oligodendrocyte processes reveals structures containing clusters of polyribosomes that correspond in approximate size and distribution to the granules reported here (unpublished observations).

Similar granules may be present in other cell types but difficult to visualize except under certain conditions. In a typical cell, granules in the perikaryon may be too densely packed to resolve as separate entities. In the oligodendrocyte, the cytoplasm is dispersed in a thin layer which, in combination with the optical sectioning capability of the confocal microscope, facilitates resolution of individual granules. Furthermore, MBP mRNA is expressed at relatively high levels in oligodendrocytes. A substantial proportion of the total granules in the periphery of the cell appears to contain MBP mRNA, which may also facilitate visualization by FISH. Analyzing the distribution of total mRNA, or of a less highly expressed mRNA, might reveal either too many or too few granules to resolve as discrete entities.

In this study, granules were visualized by a variety of different methods including: FISH (with both digoxigenin- and biotin-labeled probes), immunofluorescence (with a variety of different antibodies) and, in live cells, using an RNA stain. Similar-appearing granules have also been observed with

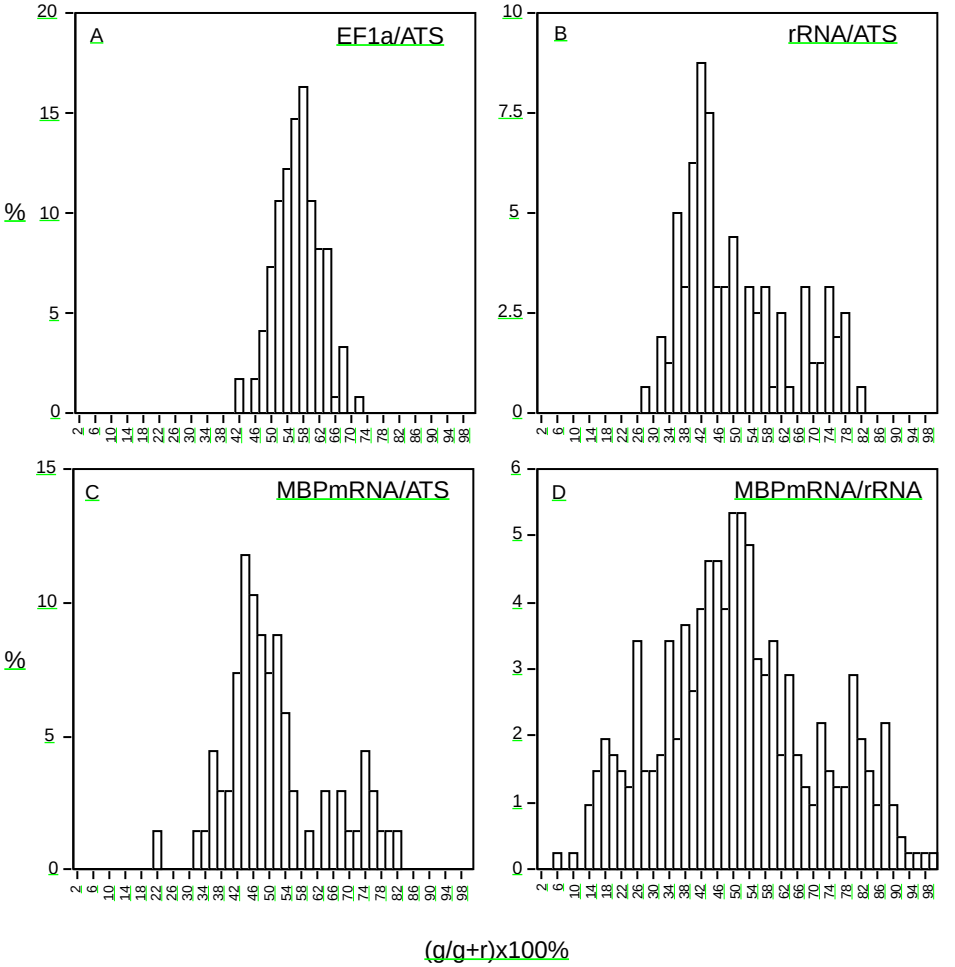

Fig. 4. Single granule ratiometric analysis of colocalization. Several hundred individual granules were selected from cells labeled as described in Fig. 1A-D. Each granule was subjected to single granule ratiometric analysis as described in Materials and Methods. The results are presented as frequency distributions. The *x*-axis shows the total granule intensity in the green channel divided by the sum of the intensities in the green and red channels expressed as a percentage. The *y*-axis shows the percentage of total granules with each ratio value. (A) Distribution of granules from cells labeled with ATS (green) and EF1a(red). (B) Distribution of granules from cells labeled with ATS (green) and rRNA (red). (C) Distribution of granules from cells labeled with ATS (green) and MBP mRNA (red). (D) Distribution of granules from cells labeled with rRNA (green) and MBP mRNA (red).

microinjected fluorophore-tagged RNA in live cells (Ainger et al., 1993). Since granules are observed with a variety of labeling techniques in both fixed and live cells, it is likely that they represent real subcellular structures and are not artifacts due to fixation or to a particular labeling technique.

Packaging components of the protein synthetic machinery into granules would be expected to increase the efficiency of protein synthesis by limiting diffusion of intermediates and by increasing the local concentrations of individual components. If protein synthesis occurs in the granules (which has not been demonstrated), this may represent the physical basis for 'channeling' of protein synthesis which was proposed on the basis of results of metabolic labeling experiments (Negrutskii and Deutscher, 1991, 1992; Negrutskii et al., 1994; Stapulionis and Deutscher, 1995). It may also explain the high rate of protein synthesis observed in eucaryotic cells despite the relatively low overall concentrations of protein synthetic components compared to procaryotes. If all of the essential components are present in granules, their local concentrations within the granules may be as high or higher than in procaryotes.

The stoichiometries of individual components in each granule are not known. Virtually all granules contain ATS and EF1a in relatively constant proportions. The majority of the granules also contain rRNA. The ribosome-deficient granules presumably represent a translationally inactive population. Some granules also lack MBP mRNA. These granules may contain other mRNAs, or may represent mRNA-deficient granules, either in the process of assembly before mRNA has become associated or in the process of disassembly after mRNA has been degraded. Exogenous MBP mRNA microinjected into oligodendrocytes forms similar-appearing granules which have been implicated in transport of the mRNA to the periphery of the cell (Ainger et al., 1993). It is likely that at least some of the endogenous MBP mRNA-containing granules observed in this study also represent transport intermediates. One possibility is that the ribosome-deficient granules (which are presumably translationally inactive) represent transport intermediates.

In the oligodendrocyte nucleus, both ATS and EF1a appear in a dispersed form while rRNA appears associated with nucleoli. The different morphological appearance of the material in the nucleus compared to the granules in the cytoplasm suggests that the nuclear ATS, EF1a and rRNA are functionally distinct from the cytoplasmic components. EF1a-like proteins have been observed in the microtubular network of sea urchin centromere spindle (Ohta et al., 1990) and EF1a has also been shown to be an actin-binding protein in *Dictyostelium* (Yang et al., 1990). Thus, nuclear EF1a may be associated with cytoskeletal elements in the nucleus. The function of nuclear ATS is not known. Nucleolar rRNA presumably represents newly sythesized transcripts bound for assembly into ribosomes.

In summary, the results presented here provide evidence that the components of the protein synthetic machinery are organized into intracellular granules. The granules in oligodendrocytes were shown to contain ATS, EF1a, rRNA and MBP mRNA, and may contain other components of the protein synthetic machinery as well. This spatial organization may increase the efficiency of protein synthesis and may also provide a vehicle for transport and localization of specific mRNAs within the cell.

This work was supported by NIH grants: NS19943 to E.B., GM23585 to D.E.K., GM16317 to M.P.D. and NS15190 to J.H.C.; and by an Elias Howe High Technology Equipment grant from the Department of Higher Education of the State of Connecticut. We thank C. Barry for technical assistance.

REFERENCES

Ainger, K., Avossa, D., Morgan, F., Hill, S. J., Barry, C., Barbarese, E. and Carson, H. (1993). Transport and localization of exogenous myelin basic protein mRNA microinjected into oligodendrocytes. *J. Cell Biol.* **123**, 431-441.

Barbarese, E., Braun, P. E. and Carson, J. H. (1977). Identification of prelarge and presmall basic proteins in mouse myelin and their structural relationship to large and small basic proteins. *Proc. Nat. Acad. Sci. USA* **74**, 3360-3364.

Barbarese, E. (1991). Spatial distribution of myelin basic protein mRNA and polypeptide in quaking oligodendrocytes in culture. *J. Neurosci. Res.* **29**, 271-281.

Bec, G., Kerjan, P., Zha, X. D. and Waller, J.-P. (1989). Valyl-tRNA synthetase from rabbit liver. I. Purification as a heterotypic complex in association with elongation factor 1. *J. Biol. Chem.* **264**, 21131-21137.

Biegel, D. and Pachter, J. S. (1991). "In vitro" translation: Use of the cytoskeletal framework to direct cell-free protein synthesis. *In Vitro Cell. Dev. Biol.* **27A**, 75-85.

Cervera, M., Dreyfuss, G. and Penman, S. (1981). Messenger RNA is translated when associated with the cytoskeletal framework in normal and VSV-infected HeLa cells. *Cell* **23**, 113-120.

Colman, D. R., Kreibich, G., Frey, A. B. and Sabatini, D. D. (1982). Synthesis and incorporation of myelin polypeptides into CNS myelin. *J. Cell Biol.* **95**, 598-608.

Dang, C. V., Yang, C. H. and Pollard, T. D. (1983). Association of methionyl-tRNA synthetase with detergent-insoluble components of the rough endoplasmic reticulum. *J. Cell Biol.* **96**, 1138-1147.

Deutscher, M. P. (1984). The eukaryotic aminoacyl-tRNA synthetase complex: suggestions for its structure and function. *J. Cell Biol.* **99**, 373-377.

Feinberg, A. P. and Vogelstein, B. (1983). A technique for radiolabeling DNA restriction endonuclease fragments to high specific activity. *Anal. Biochem.* **132**, 6-13.

Graf, H. (1977). Interaction of aminoacyl-tRNA synthetases with ribosomes and ribosomal subunits. *Biochim. Biophys. Acta* **425**, 175-184.

Holmes, E., Hernanson, G., Cole, R. and de Vellis, J. (1978). Developmental expression of glial-specific mRNAs in primary cultures of rat brain visualized by in situ hybridization. *J. Neurosci. Res.* **19**, 389-396.

Howe, J. G. and Hershey, J. W. B. (1984). Translational initiation factor and ribosome association with the cytoskeletal framework fraction from HeLa cells. *Cell* **37**, 85-93.

Irvin, J. D. and Hardesty, B. (1972). Binding of aminoacyl-tRNA synthetases to ribosomes from rabbit reticulocytes. *Biochemistry* **11**, 1915-1920.

Lenk, R., Ransom, L., Kaufmann, Y. and Penman, S. (1977). A cytoskeletal structure with associated polyribosomes obtained from Hela cells. *Cell* **10**, 67-78.

Mirande, M., Le Corre, D., Louvard, D., Reggio, H., Pailliez, J.-P. and Waller, J.-P. (1985). Association of an aminoacyl-tRNA synthetase complex and of phenylalanyl-tRNA synthetase with the cytoskeletal framework fraction from mammalian cells. *Exp. Cell Res.* **156**, 91-102.

Miseta, A., Woodley, C. L., Greenberg, R. and Robinson, I. (1991). Mammalian seryl-tRNA synthetase associates with mRNA in vivo and has homology to elongation factor 1a. *J. Biol. Chem.* **266**, 19158-19161.

Negrutskii, B. S. and Deutscher, M. P. (1991). Channeling of aminoacyl-tRNA for protein synthesis in vivo. *Proc. Nat. Acad. Sci. USA* **88**, 4991-4995.

Negrutskii, B. S. and Deutscher, M. P. (1992). A sequestered pool of aminoacyl-tRNA in mammalian cells. *Proc. Nat. Acad. Sci. USA* **89**, 3601-3604.

Negrutskii, B. S., Stapulionis, R. and Deutscher, M. P. (1994). Supramolecular organization of the mammalian translation system. *Proc. Nat. Acad. Sci. USA* **91**, 964-968.

Ohta, K., Toriyama, M., Miyazaki, M., Murofushi, H., Hosoda, S., Endo, S. and Sakai, H. (1990). The mitotic apparatus-associated 51-kDa protein from sea urchin eggs is a GTP-binding protein and is immunologically related to yeast polypeptide elongation factor 1a. *J. Biol. Chem.* **265**, 3240-3247.

Pachter, J. S. (1992). Association of mRNA with cytoskeletal framework:

its role in the regulation of gene expression. *Crit. Rev. Eukaryotic Gene Exp.* **2**, 1-18.

Roach, A., Boylan, K., Horvath, S., Prusiner, S. B. and Hood, L. E. (1983). Characterization of cloned cDNA representing rat myelin basic protein: Absence of expression in brain of shiverer mutant mice. *Cell* **34**, 799-806.

Ryazonov, A. G., Ovchinnikov, L. P. and Spirin, A. S. (1987). Development of structural organization of protein-synthesizing machinery from prokaryotes to eukaryotes. *Biosystems* **20**, 275-288.

Singer, R. H., Lawrence, J. B. and Villenay, C. (19). Optimization of in situ hybridization using isotopic and non-isotopic detection methods. *BioTechniques* **4**, 230-251.

Singer, R. H. (1992). The cytoskeleton and mRNA localization. *Curr. Opin. Cell Biol.* **4**, 15-19.

Stapulionis, R. and Deutscher, M. P. (1995). A channeled tRNA cycle during mammalian protein synthesis. *Proc. Nat. Acad. Sci. USA* **92** (in press).

Taneja, K. L., Lifshitz, L. M., Fay, F. S. and Singer, R. H. (1992). Poly(A) RNA codistribution with microfilaments: Evaluation by in situ hybridization and quantitative digital imaging microscopy. *J. Cell Biol.* **119**, 1245-1260.

Trapp, B. D., Moench, T., Pulley, M., Barbosa, E., Tennekoon, G. and Griffin, J. (1987). Spatial segregation of mRNA encoding myelin-specific proteins. *Proc. Nat. Acad. Sci. USA* **84**, 7773-7777.

Vellekamp, G. and Deutscher, M. P. (1985). A basic NH2-terminal extension of rat liver arginyl-tRNA synthetase required for its association with high molecular weight complexes. *J. Biol. Chem.* **262**, 9927-9930.

Yang, F., Demma, M., Warre, V., Dhawardhan, S. and Condeelis, J. (1990). Identification of an actin-binding protein from dictyostelium as elongation factor 1a. *Nature* **347**, 494-496.

(Received 14 March 1995 - Accepted 22 May 1995)